RSC Advances

ROYAL SOCIETY OF CHEMISTRY

www.rsc.org/advances

Journal Name

ARTICLE

CFD Simulations of Catalytic Hydrodeoxygenation of Bio-oil using Pt/Al_2O_3 in a Fixed Bed Reactor

Received 00th January 20xx,
Accepted 00th January 20xx

DOI: 10.1039/x0xx00000x

www.rsc.org/

Malladi D. Subramanyam,[a] Anjani R.K. Gollakota,[a] and Nanda Kishore[a]*

The upgradation of pyrolysis bio-oil by hydrodeoxygenation (HDO) process using Pt/Al_2O_3 catalyst is numerically investigated using a computational fluid dynamics based commercial solver, ANSYS Fluent 14.5. In the simulations fixed bed reactor with concurrent upflow of unprocessed bio-oil and H_2 gas is introduced. The dimensions of the reactor and the thermo-physical properties of all three phases are adopted from experimental data available in the literature. The size of catalyst particles is 10µm and a loading of 60g is used in the present simulations. The main aim of this work is to numerically investigate the effects of weight hourly space velocity (WHSV), temperature (T) and pressure (P) on the upgradation of bio-oil using catalytic hydrodeoxygenation and to delineate effects pertinent parameters on distribution of various products of upgraded biofuel. For this purpose following ranges of parameters considered in this work: weight hourly space velocity, WHSV = 2 – 4 h^{-1}; temperature, T = 623 K – 673 K and pressure, P = 6996 kPa – 10443 kPa. Briefly the results indicate that the lower WHSV and higher pressure are favourable for the yield of aromatics and conversion of high non-volatiles components, however effect of temperature is negligible. Finally a comparison is made on conversion of high non volatiles and phenols and yield of alkanes and aromatics obtained in fixed bed and fluidized reactors for identical values of WHSV, temperature and pressure. It is found that the performance of HDO of bio-oil by the use of Pt/Al_2O_3 catalyst in fixed bed reactor is superior in all aspects in comparison to fluid bed reactors in the present range of pertinent parameters.

Keywords: Bio-oil, Upgradation, Bio-fuel, Catalyst, Hydrodeoxygenation, CFD

Introduction

Biomass is very attractive and productive resource for energy production in the form of transportation fuels amongst all sustainable and renewable resources. It can be treated in different methods such as physical, biochemical and thermal conversion[1]. Amongst many biomasses to bio-oil conversion processes, fast pyrolysis is very propitious route and gained great interest in researchers for the conversion of the lignocellulosic biomass to liquid bio-oil. Pyrolysis process produces liquid bio-oil product with yield up to 80 wt. % on dry biomass basis. Thus obtained bio-oil from pyrolysis process contains acids, alkenes, esters, alcohols, ketones, furans, phenols, aldehydes, etc. However, such unprocessed bio-oils are not directly used as transportation fuel because of the presence of oxygenated compounds and high acidic and non-volatile nature of unprocessed bio-oils. Further such unprocessed bio-oils have adverse properties such as high viscosity, water content which may cause corrosion in the combustion chamber, low heating value and low stability[2]. The high oxygen content (≈ 30-40 wt. %) renders the usage of bio-oil because the high oxygen content makes the unprocessed bio-oil of low HNV, high ignition delay and thermal instability. Thus the bio-oils must be processed so that they can be used as transportation fuels and the available upgradation methods are classified as physical, catalytic and chemical upgrading[3]. Many of the upgrading processes such as catalytic hydroprocessing[4], esterification[5,6], catalytic pyrolysis[7,8], hydrodeoxygenation (HDO)[4,9–11], and steam reforming[12] are focused on the removal of oxygen from bio-oil. The catalytic hydro-processing has the advantage of upgrading the bio-oil to selected range of hydrocarbons at high temperature and high hydrogen pressure but it has limited deoxygenation feasibility. During the hydrotreatment processes of bio-oil several reactions occurs simultaneously such as hydrogenation, hydrogenolysis, hydrodeoxygenation, decarboxylation, decarbonylation, cracking/hydrocracking, and polymerization reactions. In HDO processes, the hydrogen is used to remove the oxygen contents in presence of catalyst to produce transportation fuels as like

[a] Department of Chemical Engineering, Indian Institute of Technology Guwahati, Assam – 781039, India.

conventional hydro-desulfurization (HDS) process where it removes sulphur, although the degree of deoxygenation is dependent on the type of pyrolysis oil used. In the initial period of research on HDO process, it was performed in similar method as conventional petroleum HDS process, but greater disparity has been observed between the two mechanisms[13]. Elliott and Baker[14] performed HDO in bench scale continuous reactor at 350-450 °C and 138 bar by using Ni-Mo/Al_2O_3 and Co-Mo/Al_2O_3 catalysts, and the yield of upgraded oil was 80 wt.% with 90 % oxygen removal. Gagnon and Kaliagiune[15] performed HDO of pyrolysis vacuum oil with ruthenium and nickel oxide and copper chromite catalyst supported by alumina in batch slurry reactor where the catalyst lead to excessive char and coke formation. Sheu et al.[16] conducted HDO of pine pyrolytic oil using platinum supported on alumina catalyst along with other conventional HDS catalysts such as Ni-Mo/Al_2O_3 and Co-Mo/Al_2O_3 at operating conditions range from 350-400 °C, 6996-10443 kPa, 0.5 – 3 h^{-1} of WHSV in a trickle bed reactor. They adopted lumped kinetic parameters in order to obtain the mass fractions obtained in the upgradation processes as groups of high non-volatiles (HNV), low non-volatiles (LNV), aromatics, phenols, etc. Elliott[17] developed a two stage up-flow packed bed HDO reactor maintaining different operating conditions on various pyrolysis oils to reduce coke formation using HDS catalysts, i.e., Ni-Mo/Al_2O_3 and Co-Mo/Al_2O_3 catalysts. The first stage stands for reduction in reactive species like ethers, methoxy phenols, aldehydes, and ketones, called as hydrotreating stage and second stage for removal of remaining oxygen compounds as hydrocracking stage.

It is known that many studies on HDO of bio-oil are conducted in continuous reactors, and only a few in batch reactors[15,18]. Oasmaa[18] carried out HDO in batch reactor using cobalt oxide on supported Al_2O_3 catalyst and achieved 86% deoxygenation. Baldauf[19] achieved 99.9 wt.% deoxygenating on HDO of pyrolysis oils in packed bed up-flow and downflow modes by using sulphided Co-Mo and Ni-Mo catalysts and operational problems such as catalyst deactivation, plugging and coking are encountered during the process. Further the major yield is water than the oil, and the so-obtained upgraded bio-oil is not suitable for direct usage. Many experiments are carried out between 1995 and 2004 on HDO of various unprocessed bio-oil feedstocks in two stage packed bed reactor by Conti[20], Samolada[21], Suping[22] in slurry reactors, and Elliott[23] in two stage trickle bed reactor using ruthenium based catalyst. The experiments on HDO has been progressed further by using noble metal catalysts, bimetallic catalysts supported by carbon, zirconium oxide, sulphided compounds, titanium oxide[24]. Parapati et al.[25] worked on single-stage catalytic hydrotreatment in a continuous packed-bed reactor using various catalysts, and reported that the catalyst deactivation and low yields are the main barriers of upgradation of bio-oil. Thus, on the basis of aforementioned literature review, it can be concluded that extensive research has to be carried out on HDO of various pyrolysis oil feedstocks, catalyst functions, and reactor specifications for minimizing coke, optimizing process economy, and maximizing the yields. In the present study, numerical results are presented on upgradation of bio-oil in concurrent upflow fixed bed reactor using catalytic HDO to convert unprocessed bio-oil into lighter hydrocarbons such as gasoline and diesel. The conversion of HNV and phenols; and yield of alkanes and yield of alkanes and aromatics obtained in fixed bed and fluid bed reactors for identical operating conditions are compared which justifies the superiority of upflow fixed bed reactor for the HDO of pyrolytic oil using Pt/Al_2O_3 catalyst.

Problem Statement and Mathematical Formulation

A cylindrical reactor of dimensions 0.813m height and 0.0156m diameter is considered in the present study (Figure 1). The dimensions of the present simulation study are same as that of experimental work due to Sheu et al.[16] though the mode of operations are different. Sheu et al.[16] used trickle bed reactor wherein the bio-oil enters the reactor from the top and H_2 gas enter from the bottom of the reactor in which a catalyst bed along with some inert packing material are present. However in the present work, the reactor is operated in concurrent upflow fixed bed reactor mode where both the bio-oil and H_2 gas concurrently enter from the bottom of the reactor wherein 60g of Pt/Al_2O_3 catalyst bed is filled. To be specific, Pt/Al_2O_3 catalyst of 10 µm size with density of 21450 kg/m^3 are packed up to maximum packing height (0.508m) of the reactor. The 60g catalyst is charged in to the reactor corresponds to a volume fraction of 0.0286.

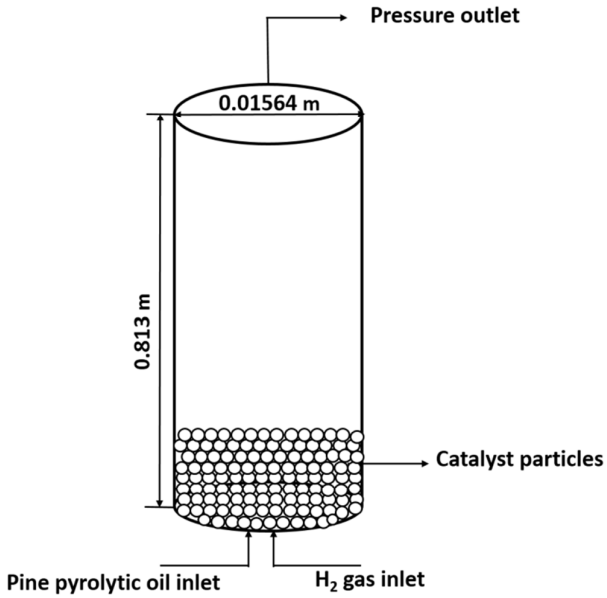

Figure 1 Schematic representation of upflow fixed bed reactor for bio-oil upgradation.

The pine pyrolytic oil consisting of various lumped groups such as heavy nonvolatile (HNV) components, light nonvolatile (LNV) components, phenols, alkanes and aromatics along with hydrogen (H_2) gas are introduced from the bottom of the reactor to pass through the catalyst bed. The thermo-physical properties of all

three phases used in the present simulations are adopted from Ref.[34-37, 39-40] and a summary of these properties is given in Table 1. The reaction pathway (adopted from Sheu et al.[16]) is shown in Figure 2 and the corresponding details of rate expressions are highlighted in Table 2. In this table ρ_1, ρ_2, ρ_3, and ρ_4 are the densities of HNV, LNV, phenols and alkane aromatics respectively. The initial compositions of all components are given in Table 3. The oil feed rate and its velocity is controlled on the basis of weight hourly space velocity (WHSV) values which is defined as gram of pine pyrolytic oil input per hour per gram of catalyst load into the reactor. For different values of WHSV, corresponding flow rates/velocities of bio-oil and H_2 gas are presented in Table 4.

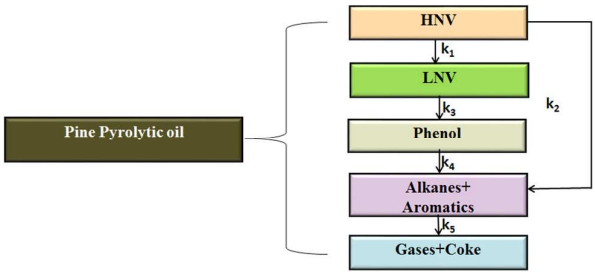

Figure 2 Reaction pathway of hydroprocessing of pine pyrolytic oil[16].

The modeling of this bio-oil upgradation process is governed by the hydrodynamics and reactions amongst the various phases involved in the process. The simulation was performed by solving the governing equations of mass, momentum and energy conservation using CFD software ANSYS Fluent 14.5. An Eulerian multiphase turbulence model is used to simulate the hydrodynamics, heat transfer, and kinetics of bio-oil in fixed bed reactor. All three phases are treated with interpenetrating continuum approach. The governing equations for hydrodynamics and the kinetic details of reactions which are adopted in the present simulations are presented below.

Hydrodynamics

The mass conservation equations of both primary (q) and secondary phases (p) can be written as:

$$\frac{1}{\rho_{rq}}\left(\frac{\partial}{\partial t}\left(\alpha_q\rho_q\right)+\nabla.\left(\alpha_q\rho_q\vec{v}_q\right)=\sum_{p=1}^{n}\left(m_{pq}-m_{qp}\right)\right) \quad (1)$$

where ρ_{rq} is the phase reference density, or the volume averaged density of q^{th} phase, $\vec{v}_q$ is the velocity of phase q and m_{pq} characterizes the mass transfer from p^{th} to q^{th} phases, and similarly m_{qp} characterizes the mass transfer from phase q to phase p.

The effective density of phase q is given as:

$$\hat{\rho}_q = \alpha_q\rho_q \quad (2)$$

where α_q is volume fraction of phase q, ρ_q is the physical density of phase q.

Table 1: Properties of three phases used in the present simulations adopted from literature.

Phase	Compound	Density (kg/m^3)	Viscosity (kg/ms)	Specific Heat (J/kg K)	Thermal Conductivity (W/m K)
Pine pyrolytic oil	HNV-(Limonene)[34]	841.15	0.00092	1833.817	0.127
	LNV-(Heptane)[35]	679.5	0.00040	2223.19	0.140
	Phenols-(Cresol-o)[39]	1030	0.18423	1430.00	0.190
	Aromatics-(Xylene)[40]	880	0.00081	1699.84	0.131
	Alkane-(Methane)[37]	0.669	0.000018	2222	0.033
H_2 gas Phase	H_2 (Gas)[37]	0.8189	0.000008	14283	0.167
	Water Vapour[37]	0.5542	0.000013	2014	0.0261
Catalyst	Pt/Al_2O_3[36]	21450	0.000017	130	71.6
	Coke +Ash[37]	375	1.206	850	0.2

Table 2 Reaction pathway and kinetic parameters adopted from Sheu et al.[16]

Reaction Pathway	Rate expression	Activation Energy, E_a (J/ kmol)	Arrhenius Constant, A (min^{-1})
$HNV \xrightarrow{k_1} LNV$	$r_1 = -k_1\rho_1$	7.40 e+ 07	3860
$HNV \xrightarrow{k_2} Alkane + Aromatics$	$r_2 = k_1\rho_1 - k_2\rho_2 - k_3\rho_2$	9.18 e+ 07	75400
$LNV \xrightarrow{k_3} Phenol$	$r_3 = k_3\rho_2 - k_4\rho_3$	8.06 e+ 07	8300
$Phenol \xrightarrow{k_4} Alkane + Aromatic$	$r_4 = k_2\rho_2 + k_4\rho_3 - k_5\rho_4$	6.23 e+ 07	950
$Alkane + Aromatic \xrightarrow{k_5} Coke + Gases + Water$	$r_5 = k_5\rho_4$	6.96 e+ 07	4000

Table 3 Initial mass fractions of all components used in the simulation studies.

Component	Mass Fraction
HNV	0.4932
LNV	0.369
Phenols	0.1232
Alkane +Aromatics	0.0146
Gases + Coke	0

Table 4 Velocity values used in the simulations for different values of WHSV in both fixed and fluidized bed reactors.

	Fixed bed	Fluid bed
WHSV (h^{-1})	2	
Oil flow rate (g/min)	120	120
Oil velocity (m/s)	1.752×10^{-4}	1.752×10^{-4}
Gas velocity (m/s)	0.01752	0.047
	Fixed bed	Fluid bed
WHSV (h^{-1})	3	
Oil flow rate (g/min)	180	180
Oil velocity (m/s)	2.604×10^{-4}	2.604×10^{-4}
Gas velocity (m/s)	0.026	0.047
	Fixed bed	Fluid bed
WHSV (h^{-1})	4	
Oil flow rate (g/min)	240	240
Oil velocity (m/s)	3.437×10^{-4}	3.437×10^{-4}
Gas velocity (m/s)	0.0346	0.047

Table 5 Momentum exchange coefficient (Schiller-Neumann[26] drag functions) for fluid phase.

$$\overline{\overline{\tau_q}} = \alpha_q\mu_q\left(\nabla\overrightarrow{v_q} + \nabla\overrightarrow{v_q}^T\right) + \alpha_q\left(\lambda_q - \frac{2}{3}\mu_q\right)\nabla.\overrightarrow{v_q}\overline{\overline{I}}$$

$$K_{pq} = \frac{\alpha_q\alpha_p\rho_p f}{\tau_p}$$

$$\tau_p = \frac{\rho_p {d_p}^2}{18\mu_q}$$

$$f = \frac{C_D Re}{24}$$

$$C_D = \left\{\frac{24(1 + 0.15Re^{0.687})}{Re}\right\} \text{ for } Re \le 1000$$

$$C_D = 0.44 \text{ for } Re > 1000$$

$$Re_{pq} = \frac{\rho_q\left|\overrightarrow{v_p} - \overrightarrow{v_q}\right|d_p}{\mu_q}$$

The conservation of momentum equation for a fluid phase (primary phase 'q' = liquid & gas) is

$$\frac{\partial}{\partial t}\left(\alpha_q\rho_q\overrightarrow{v_q}\right) + \nabla.\left(\alpha_q\rho_q\overrightarrow{v_q}\overrightarrow{v_q}\right) = -\alpha_q\nabla p + \nabla.\overline{\overline{\tau_q}} + \sum_{p=1}^{n}\left(\begin{matrix}K_{pq}\left(\overrightarrow{v_p} - \overrightarrow{v_q}\right) \\ +m_{pq}\overrightarrow{v_{pq}} - m_{qp}\overrightarrow{v_{qp}}\end{matrix}\right) + \alpha_q\rho_q\vec{g} + \left(\overrightarrow{F_q}\right) \quad (3)$$

The momentum exchange coefficients from Schiller-Neumann[26] drag correlation for fluid phase are given in Table 5.

The conservation of momentum for the s[th] solid phase is

$$\frac{\partial}{\partial t}\left(\alpha_s\rho_s\overrightarrow{v_s}\right) + \nabla.\left(\alpha_s\rho_s\overrightarrow{v_s}\overrightarrow{v_s}\right) = -\alpha_s\nabla p - \nabla p_s + \nabla.\overline{\overline{\tau_s}} + \alpha_s\rho_s\vec{g} + \sum_{l=1}^{n}\left(K_{ls}\left(\overrightarrow{v_l} - \overrightarrow{v_s}\right) + m_{ls}\overrightarrow{v_{ls}} - m_{sl}\overrightarrow{v_{sl}}\right) \quad (4)$$

The kinetic theory of granular flow, which considers the conservation of solid fluctuation energy, was used for closure of the solids stress terms. The transport equation from the kinetic theory from Gidaspow and Ding[27] is

$$\frac{3}{2}\left[\frac{\partial}{\partial t}(\rho_s\alpha_s\theta_s) + \nabla.(\rho_s\alpha_s\theta_s\overrightarrow{v_s})\right] = \left(-p_s\overline{\overline{I}} + \overline{\overline{T}}\right):\nabla\overrightarrow{v_s} + \nabla.\left(K_{\theta_s}\nabla\theta_s\right) - \gamma\theta_s + \emptyset_{ls} \quad (5)$$

Table 6 presents the Gidaspow model[28], which is a combination of Wen and Yu[29] and Ergun[30] drag model equations for a solid phase; whereas Table 7 represents the granular temperature and solids pressure for solid phase from Lun[31].

Table 6 Momentum exchange coefficient (Wen and Yu[29], Ergun[30] drag functions) for solid phase

$$K_{ls} = C_D\frac{3}{4}\rho_l\frac{\alpha_l\alpha_s}{d_s}\left|\vec{v}_s - \vec{v}_l\right|\alpha_l^{-2.65} \quad \text{for} \quad (\alpha_l > 0.8)$$

$$K_{ls} = \frac{150\alpha_s(1\text{-}\alpha_l)\mu_l}{\alpha_l {d_s}^2} + \frac{1.75\alpha_s\rho_l\left(\vec{v}_s - \vec{v}_l\right)}{d_s} \text{ for } (\alpha_l \le 0.8)$$

$$C_D = \frac{24}{\alpha_l Re_s}\left(1 + 0.15\left(\alpha_l Re_s\right)^{0.687}\right)$$

$$Re_s = \frac{\rho_l d_s\left|\vec{v}_s - \vec{v}_l\right|}{\mu_l}$$

Table 7 Granular temperature and solids pressure (Lun[31]) for solid phase

$$K_{\theta_s} = \frac{150\rho_s d_s\sqrt{\theta\pi}}{384(1+e_{ss})g_{0,ss}}\left[1+\frac{6}{5}\alpha_s g_{0,ss}(1+e_s)\right]^2$$
$$+2\rho_s\alpha_s^2 d_s(1+e_{ss})g_{0,ss}\sqrt{\frac{\theta_s}{\pi}}$$
$$\mathrm{P_s} = \rho_s\alpha_s\theta_s\left(1+2(1+\mathrm{e_{ss}})\mathrm{g_{0,ss}}\alpha_s\right)$$
where $g_0(\varepsilon) = \left(1-\left(\frac{\alpha_s}{\alpha_{s,\max}}\right)^{\frac{1}{3}}\right)^{-1}$

Table 8 Interaction energy equations for fluid-fluid (Ranz and Marshall[32]) and for fluid-solid interactions (Gunn[33])

$$Q_{pq} = h_{pq}(T_p - T_q)$$
$$h_{pq} = \frac{6c_q\alpha_p\alpha_q Nu_p}{d_p^2}$$
$$Nu_p = 2.0 + 0.6Re_p^{1/2}Pr^{1/3}$$
$$Nu_s = \left(7-10\alpha_f+5\alpha_f^2\right)\left(1+0.7Re_s^{0.2}Pr^{1/3}\right)$$
$$+\left(1.33-2.4\alpha_f+1.2\alpha_f^2\right)Re_s^{0.7}Pr^{1/3}$$

The solid shear viscosity, μ_s is expressed as

$$\mu_s = \frac{4}{5}\alpha_s\rho_s d_s g_0(1+e_{ss})\sqrt{\frac{\theta}{\pi}}$$
$$+\frac{5\sqrt{\pi}}{48}\frac{\rho_s d_s}{(1+e_{ss})g_0}\left(1+\frac{4}{5}(1+e_{ss})g_{o,ss}\alpha_s\right)^2\sqrt{\theta} \quad (6)$$

The solid bulk viscosity, λ_s is given as

$$\lambda_s = \frac{4}{3}\alpha_s\rho_s d_s g_{0,ss}(1+e_{ss})\sqrt{\frac{\theta}{\pi}} \quad (7)$$

Generally the multiphase flow system operates under highly turbulent flow conditions. It is thus important to use the appropriate turbulence model to describe the effect of fluctuations of velocities and scalar variables for basic conservative equations. In this study, k-**ε** turbulence model is used to describe the turbulence motion in liquid phase. The turbulence kinetic energy, k, and its rate of dissipation, ε, are obtained from the following transport equations:

$$\frac{\partial}{\partial t}(\rho k)+\frac{\partial}{\partial x_i}(\rho k u_i) = \frac{\partial}{\partial x_j}\left[\left(\mu+\frac{\mu_t}{\sigma_k}\right)\frac{\partial k}{\partial x_j}\right] \quad (8)$$
$$+G_k+G_b-\rho\dot{o}-Y_M+S_k$$
$$\frac{\partial}{\partial t}(\rho\dot{o})+\frac{\partial}{\partial x_i}(\rho\dot{o}u_i) = \frac{\partial}{\partial x_j}\left[\left(\mu+\frac{\mu_t}{\sigma_{\dot{o}}}\right)\frac{\partial\dot{o}}{\partial x_j}\right]+ \quad (9)$$
$$C_{1\dot{o}}\frac{\dot{o}}{k}(G_k+C_{3\dot{o}}G_b)-C_{2\dot{o}\rho}\frac{\dot{o}^2}{k}+S_{\dot{o}}$$

where Y_M represents the contribution of the fluctuating dilation, G_b represents the generation of turbulent kinetic energy due to buoyancy, G_k represents the generation of turbulent kinetic energy due to mean velocity gradients, $C_{1\epsilon}$, $C_{2\epsilon}$, $C_{3\epsilon}$ are the constants with the values of 1.44, 1.92, 0.09; σ_ϵ, σ_k are the turbulent Prandtl numbers for k, ε with values of 1.0, 1.3 respectively; and S_k and $S_\epsilon$are the user defined source terms.

Heat transfer model

Conservation of energy in Eulerian multiphase flows, is written as

$$\frac{\partial}{\partial t}\left(\alpha_q\rho_q h_q\right)+\nabla.\left(\alpha_q\rho_q h_q\overrightarrow{u_q}\right) = -\alpha_q\frac{\partial p_q}{\partial t}+$$
$$\overline{\overline{\tau}}_q:\nabla\overrightarrow{u_q}-\nabla.\overrightarrow{q_q}+S_q+\sum_{p=1}^{n}\left(Q_{pq}+m_{pq}h_{pq}-m_{qp}h_{qp}\right) \quad (10)$$

where h_q is the specific enthalpy of q^{th} phase, $\overrightarrow{q_q}$ is the heat flux, S_q is the source term that includes the sources of enthalpy (e.g., due to chemical reaction or radiation), Q_{pq} is the intensity of heat exchange between p^{th} and q^{th} phases and h_{pq} is the interphase enthalpy. Table 8 gives the energy equations for the respective phases from Ranz-Marshall[32] and Gunn[33] models.

Kinetic model:

The finite rate/eddy dissipation model is used to study reaction kinetics of HDO of pyrolysis bio-oil. This model helps in computing both the Arrhenius rate and mixing rate.
The i^{th} species transport equation is

$$\frac{\partial}{\partial t}(\rho Y_i)+\frac{\partial}{\partial x_j}(\rho u_j Y_i) = \frac{\partial}{\partial x_j}\left(\rho D_i\frac{\partial Y_i}{\partial x_j}\right) \quad (11)$$
$$+R_i+S_i$$

where Y_i is the mass fraction of chemical species i, D_i is the diffusion coefficient, R_i is the net rate of production of species i by chemical reaction, and S_i is a source term. Since there are many species present in both pine pyrolytic oil and its hydrotreated products, the lumping of their constituents together with similar functional groups is a useful approach for studying reaction kinetics. Also lumped kinetic models give a useful insights and clear

understanding in order to quantify the effects of process variables on product yields. Therefore in this work, lumping kinetic models of hydrodeoxygenation of pyrolytic bio-oil proposed through experimental means by Sheu et al.[16] are used and their reaction mechanism of lumped parameter model is adopted in the present simulation work. The schematic representation of their reaction pathway of hydro-processing of bio-oil is shown in Figure 2.

Numerical methodology

Aforementioned governing equations along with other supporting models are solved in two dimensional computational domain using commercial CFD based software ANSYS Fluent[37]. The dimensions of the reactor used in the simulation are same as experimental setup of Sheu et al.[16] Grids inside the reactor domain are generated using Gambit 2.2.30 and exported to Fluent 14.5 software. The 2D computational structured hexahedral grid was discretized by 6000 quadrilateral cells, 12170 faces with 7000 node points. The bottom inlet of the reactor is designated as "velocity inlet" boundary in Fluent software[37]. At the inlet, the velocities, mass fractions, volume fractions, temperatures of the three phases along with temperature and pressure are specified according to the desired operating conditions. The outlet at the top of the reactor is set as "pressure outlet" boundary. The other boundary conditions are specified as "wall" boundaries which are defined as no-slip boundaries for all phases. In Fluent, phase coupled semi-implicit method for pressure linked equations (PC-SIMPLE) algorithm which is an extension of SIMPLE algorithm is adopted. In order to solve a vector equation of velocity components of three phases simultaneously, a block algebraic multigrid scheme is adopted. A second order upwind scheme is used for spatial discretization whereas QUICK scheme is used for volume fractions. Finally simulations are run with a time step of 0.001s with 20 iterations per time step achieves convergence. The convergence criterion of 10^{-3} is chosen for residual components. Once the steady state for volume fractions, bed height, and conversions are achieved, then these are further utilized to analyse effects of pertinent parameters on volume and mass fractions of all components. However, before presenting new results it is required to establish the reliability of the solver by comparing the simulation results with existing experimental results. Thus the methodology used in the present study is validated with the existing experimental literature values of the mass fractions of the five lumped species[16] hydrodeoxygenation in a fixed bed mode and presented elsewhere[38]. In this comparison, it was observed that the mass fractions of components obtained by this simulation study are in good agreement with the experimental mass fractions of all components except the amount of coke formed. The coke formation due to secondary reactions i.e., enhanced polymerization of oxy-organic compounds of bio oil species in the experiments of Sheu et al.[16] is 0.1587 when T = 673 K, P = 8720 kPa and WHSV = 2 h^{-1}. However, the present simulations show the lower mass fractions of coke formation i.e., 0.000169 at these values of independent variables under fixed bed mode of operation. The obtained aromatic content from the present CFD simulated data is in close proximate to literature value of aromatic contents[16]. This inspires confidence in the reliability and accuracy of the present numerical methodology to extent this solution method to wider range of operating conditions of HDO of pyrolytic oil using Pt/Al_2O_3 catalyst.

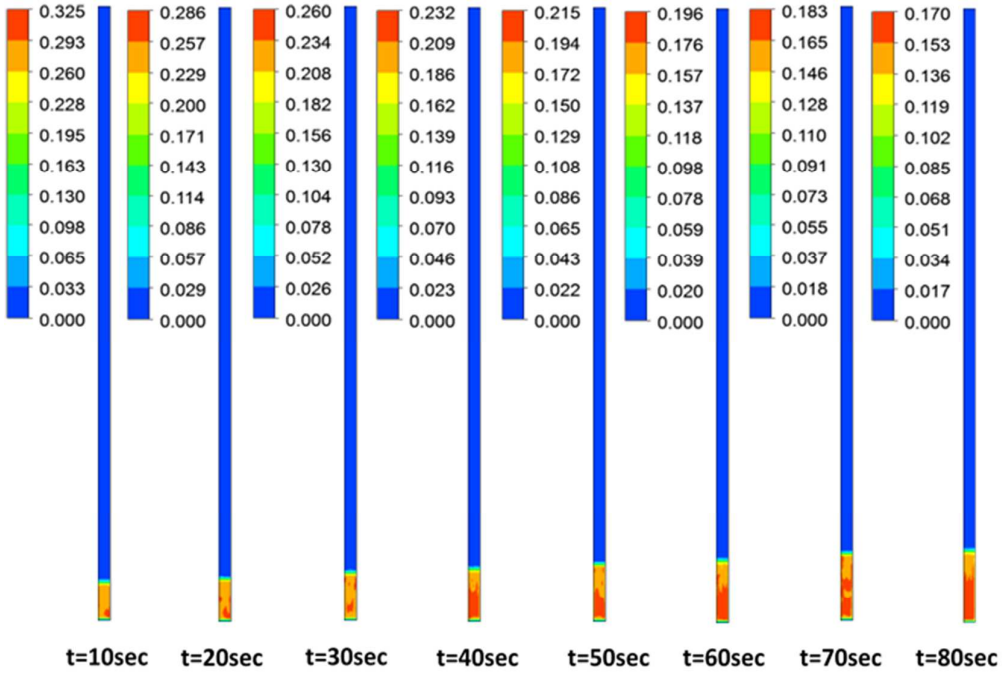

Figure 3 Volume fraction of Pt/Al_2O_3 catalyst phase at T = 673 K, P = 6996 kPa and WHSV=2 h^{-1} in a fixed bed reactor.

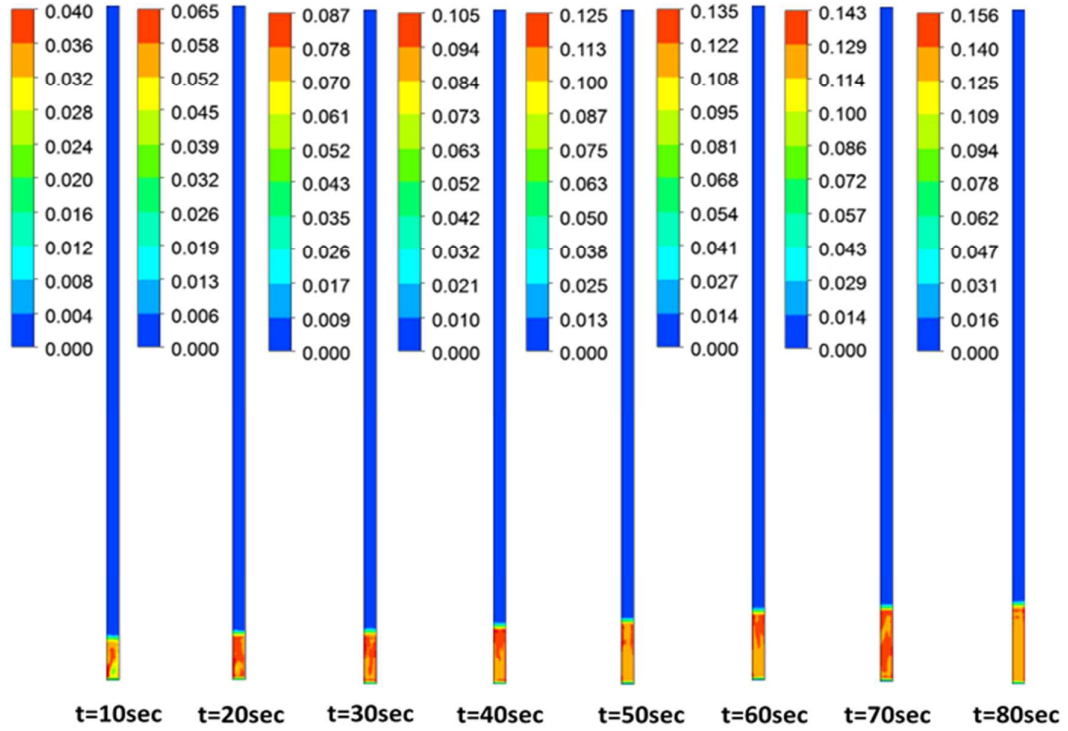

Figure 4 Volume fraction of pine-oil phase at T = 673 K, P = 6996 kPa and WHSV=2 h^{-1} in a fixed bed reactor.

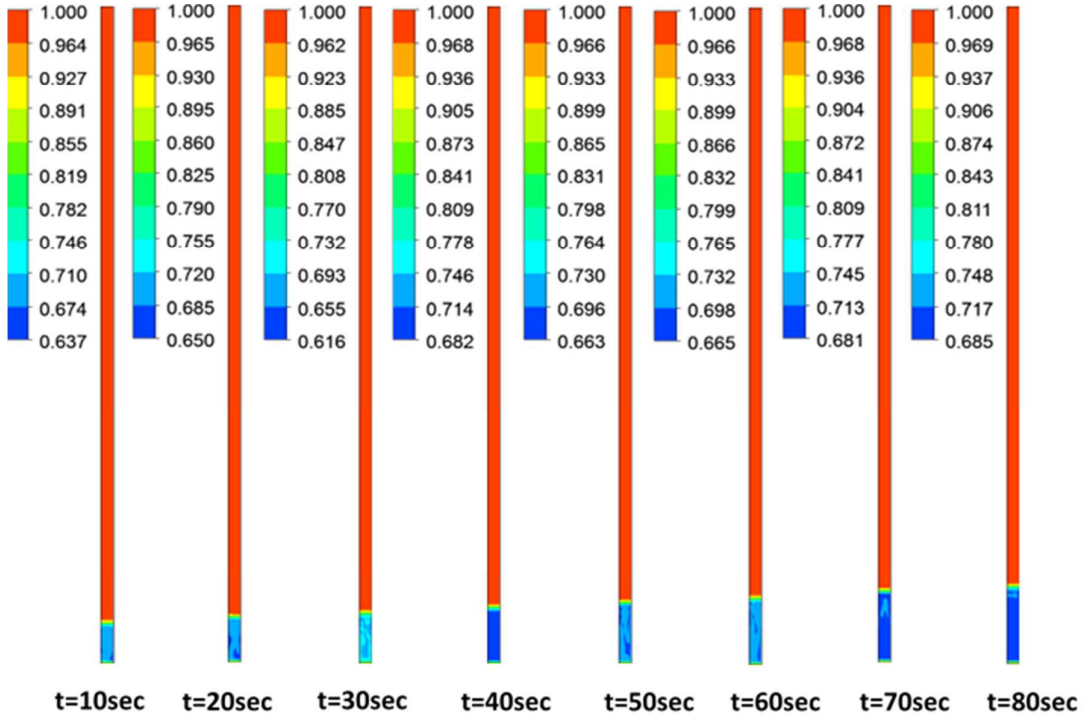

Figure 5 Volume fraction of H_2 gas phase at T = 673 K, P = 6996 kPa and WHSV=2 h^{-1} in a fixed bed reactor.

Results and Discussion

Volume Fraction of Three Phases

The variations in the volume fractions of catalyst, bio-oil and H_2 gas with respect to the time are presented in Figures 3 – 5 respectively for conditions of WHSV = 2 h^{-1}, T = 673 K and P = 6996 kPa. In the present simulation study, the oil phase and H_2 gas are upflowing through a catalyst bed and the flow conditions are maintained such that the catalyst bed should not undergo fluidization. Because in the numerical simulations it is not possible to fix the catalyst bed as is possible in experiments, the bed in the present simulations are slightly expanded as the simulation time progresses from 10s to 80s because of upflow of bio-oil phase and H_2 gas phase. The bio-oil phase is almost completely occupied the interstitial spaces available inside the catalyst bed (Figure 3). This bio-oil phase is also slightly expanding with the increase of the simulation time; however, no portion of bio-oil occupies the free board space available in the reactor. This indicates that through the reaction time (until the steady state is established) the bio-oil phase is in excellent contact with the catalyst bed and it also interact with the upflowing H_2 gas so that efficient HDO process takes place inside the bed. As can be seen in Figure 5, the H_2 gas mostly occupies the interstitial spaces available between the catalyst particle along with the bio-oil phase up to the simulation time of t = 30 s. However as the time progresses further it gradually enters the free board space along with other gaseous and vapor products formed during the HDO process. Therefore it is judicious to select the WHSV values (oil flow rate and catalyst loading) and H_2 gas flow velocity such that the intimate contact between three phases exist for longer time so that the conversion of unprocessed bio-oil in to bio-fuel can effectively take place.

The volume fraction images of three phases with respect to the simulation time for other combinations of WHSV, T and P are qualitatively similar as shown in Figures 3 – 5; hence are not repeated herein. However, their final steady values against various combinations of these pertinent parameters such as WHSV, T and P are presented in Figure 6. The values of volume fractions of three phases presented in Figure 6 are obtained after the steady process is established, i.e., after the cease of change in compositions of lumped components of bio-oil. From this figure, it can be see that the slight expansion of catalyst bed occurred only at WHSV = 2 h^{-1} and T = 623 K as the pressure increases; however, at WHSV = 2 h^{-1} and T = 648 K, the bed is unaffected by the pressure whereas at WHSV = 2 h^{-1} and T = 678 K, the bed is found to fluctuate with the pressure. On the other hand, at WHSV = 3 h^{-1} and WHSV = 4 h^{-1}, the catalyst bed volume fraction is unaffected by the variations in temperature and pressure because of decreasing residence time with the increasing WHSV; however, for a fixed combination of temperature and pressure, the volume fraction of catalyst phase decreases with the increasing WHSV. In the case of bio-oil volume fraction, at WHSV = 2 h^{-1} and for low value of pressure, i.e., at P = 6996 kPa, the effect of temperature is negligible; however, as the pressure increases to P = 8720 kPa and P = 10443 kPa, the volume fraction of bio-oil increases with the temperature. By increasing the WHSV to 3 h^{-1}, the volume fraction of bio-oil increases with pressure for temperatures of T = 648 K and T = 673 K but unaffected by pressure if T = 623 K. However, interestingly at WHSV = 4 h^{-1} (i.e., small residence time compared to other two values of WHSV), mixed trends in volume fraction of bio-oil are observed with respect to temperature for all values of pressure. The reason ascribed for the mixed trend with rising temperatures is due to the enhanced polymerization of oxy-organics which are precursors for the coke formation and rises with the rise in temperature. As the temperature rises the aromatic condensation followed by hydrogenation reaction takes place leading to the asymmetrical behaviour. For H_2 gas case, its volume fraction increases with increasing WHSV values irrespective of the combination of temperature and pressure; however, for a fixed value of WHSV, the H_2 volume fraction shows a mixed behaviour with both temperature and pressure except for the case of WHSV = 4 h^{-1} and P = 10444 kPa, it is unaffected by the variations in the temperature.

Steady Mass Fractions of Lumped Components

Figure 7 present the mass fractions of HNV component in the final bio-fuel after cease of HDO process because of establishment of steady state for different combinations of WHSV, T and P. For all values of WHSV and T, it can be seen from this figure that the mass fraction of HNV decreases with the increasing pressure. For fixed combinations of pressure and temperature, it decreases with increasing WHSV; however, mixed trends against temperature are observed for fixed values of WHSV and P. The fluctuations/ mixed trends are ascribed due to the formation of low boiling fractions through carbon bond breakage, along with hydrodeoxygenation process. Figure 8 presents the steady mass fractions of LNV for different operating values of WHSV, T and P. Qualitatively similar functionality of LNV against WHSV, T and P are seen as in the case of HNV mass fractions, i.e., mass fraction of LNV decreases with increasing pressure and decreasing WHSV values while mixed trends observed with respect to temperature. Since non-volatile components are undesirable components in the fuel, it is suggested that the HDO process should run at higher pressure and lower WHSV values. Figure 9 shows the mass fractions of phenol in the final pyrolytic bio-fuel present in the reactor after steady state for various values of WHSV, T and P. For WHSV = 2 h^{-1} and 3 h^{-1}, the phenol mass fractions are increasing with the pressure and mixed trends are seen against temperature values. This may be due to the fact that phenols are very much resistant to the hydrodeoxygenation because the bond strength of oxygen atoms is high. Further increasing WHSV leads to the slow conversion of phenols to the alkane and aromatic species but with small conversion rates. For WHSV = 4 h^{-1}, the phenols mass fraction decreasing with pressure for T = 623 K and 648 K; however, for T = 673 K, mass fractions of phenols is maximum at P = 8720 kPa than at P = 6996 kPa and P = 10444 k Pa. In such kind of HDO processes, the phenols are intermediate components which are produced from HNV and are often deoxygenated in to aromatics which are

favourable components in fuels. Figure 10 shows the effects of WHSV, T and P on mass fractions of aromatics present in the final pyrolytic bio-fuel in the reactor at steady state. It can be seen from this figure that the mass fractions of aromatics substantially increase with the increasing pressure and slightly increase with the increasing WHSV values. However, the effect of temperature is insignificant for all values of WHSV and pressure. Thus in order to increase desirable aromatics in the final bio-fuel, it would be beneficial to operate HDO at higher pressures.

Comparison of Conversion and Yield in Fixed Bed and Fluid Bed Reactors

During the hydrodeoxygenation process heavy non volatiles (HNV) converted into small fractions such as LNV, phenols, to required aromatics; thus it is required to analyse the effects of operating conditions on conversion and yield of certain components. The conversion of HNV and yield of alkanes and aromatics are obtained by the use of following definitions:

$$\text{Conversion (HNV)} = \frac{\text{reactant mass fraction at inlet} - \text{reactant mass fraction at outlet}}{\text{reactant mass fraction at inlet}}$$

$$\text{Yield (Alkane and Aromatics)} = \frac{\text{amount of product formed}}{\text{amount of reactant consumed}}$$

The details of simulations of HDO in fluid bed reactor are available elsewhere[38] and some of those results are adopted here in Figures 10-12 for comparison purpose. Figure 11 shows the conversion of HNV at different values of WHSV, T and P in fixed bed and fluid bed reactors. It can be seen from this figure that the conversion of HNV is less in fluid bed reactor in comparison with fixed bed reactor and is unaffected by the operating conditions. However, in the case of fixed bed reactors, the conversion of HNV substantially increases with increasing pressure and slightly increases with the temperature; but it slightly decreases with the increasing WHSV for all values of temperature and pressures in the fixed bed reactor. Figure 12 presents the effects of WHSV, T and P on the conversion of phenols in fixed bed and fluid bed reactors; and here too the conversions are less in fluid bed reactors and are unaffected by the operating conditions. But in the case of fixed bed reactors, the phenol conversion increases with the pressure for fixed values of WHSV and temperature. However, for fixed temperature and pressure, it decreases with increasing WHSV; whereas mixed trends are seen against temperature for fixed values of WHSV and pressure. Figure 13 present effects of operating conditions on the yield of alkanes and aromatics in fixed bed and fluid bed reactors; and here too the yield is very poor in the case of fluid bed reactor which is least affected by the operating conditions. In the case of fixed bed reactor, the yield of alkanes and aromatics significantly increase with the increasing pressure and unaffected by the values of WHSV and temperatures. Finally Table 9 presents the mass fractions of all components after upgradation for all combinations of the temperature, pressure and WHSV values. Though the mass fractions of HNV, LNV, phenols and alkanes and aromatics are presented in Figures 7 – 10, respectively, the remaining fractions of coke+H2O+gases are presented in Table 9. It can be seen from this table that for a given value of WHSV, these remaining increases with the increasing temperature and pressures; whereas for a fixed combination of temperature and pressure, as the value of WHSV increases, the remaining fraction decreases. In Summary, it is understood from the simulation study that the hydrodeoxygenation of the pine pyrolytic using Pt/Al_2O_3 in the upflow fixed bed reactor favours the higher yields of alkanes and aromatics at the pertinent operating conditions. The fluidized bed perhaps fails to achieve higher solid conversion probably due to high back mixing of solid catalyst particles.

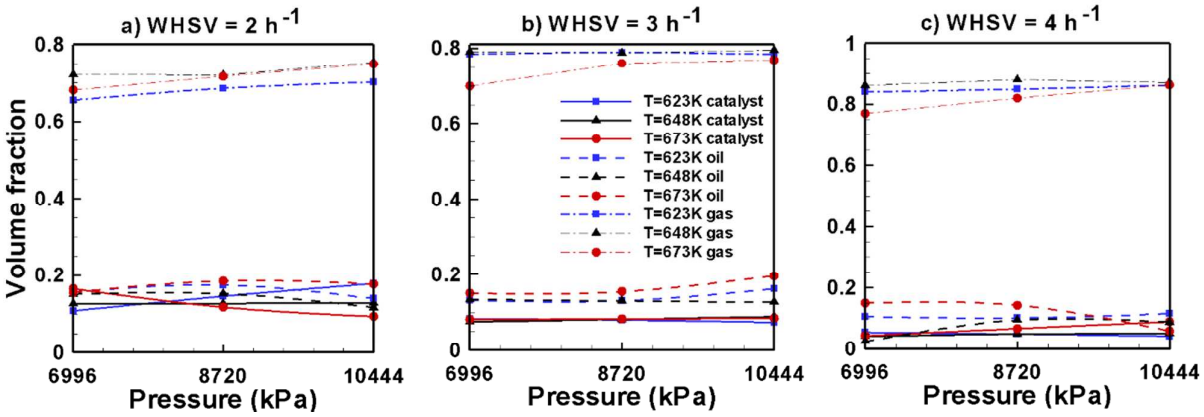

Figure 6 Steady volume fraction values of pine oil, H_2 gas and Pt/Al_2O_3 catalyst at different temperatures, pressures and WHSV values.

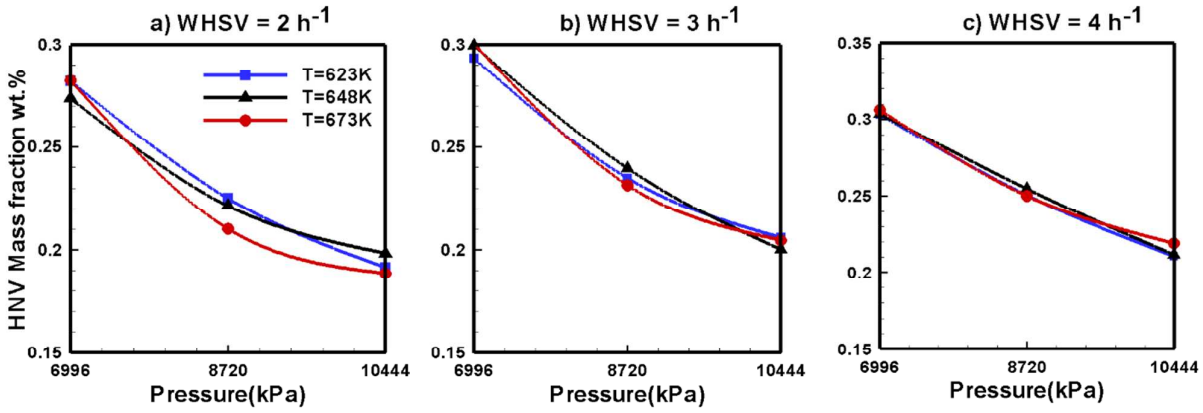

Figure 7 Final steady mass fractions of HNV in the upgraded pine-oil obtained in a fixed bed reactor in the presence of Pt/Al_2O_3 catalyst.

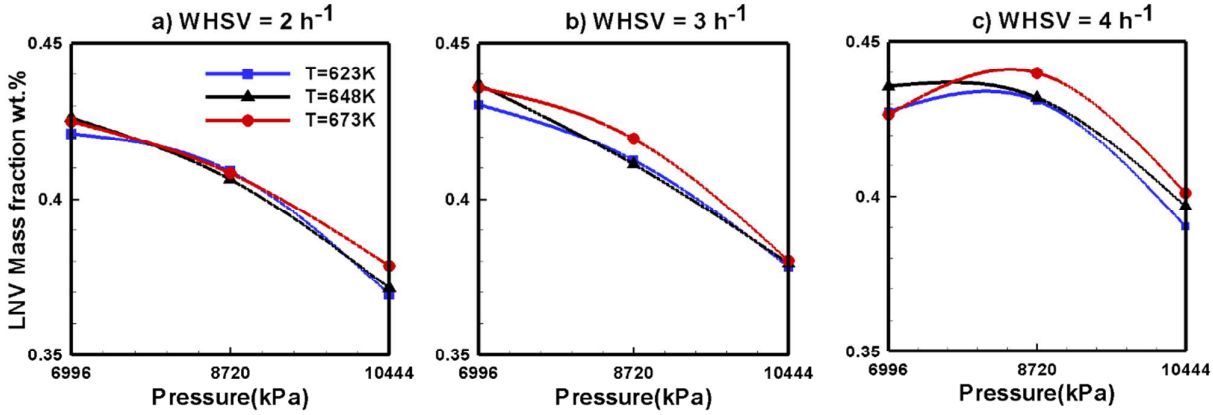

Figure 8 Final steady mass fractions of LNV in the upgraded pine-oil obtained in a fixed bed reactor in the presence of Pt/Al_2O_3 catalyst.

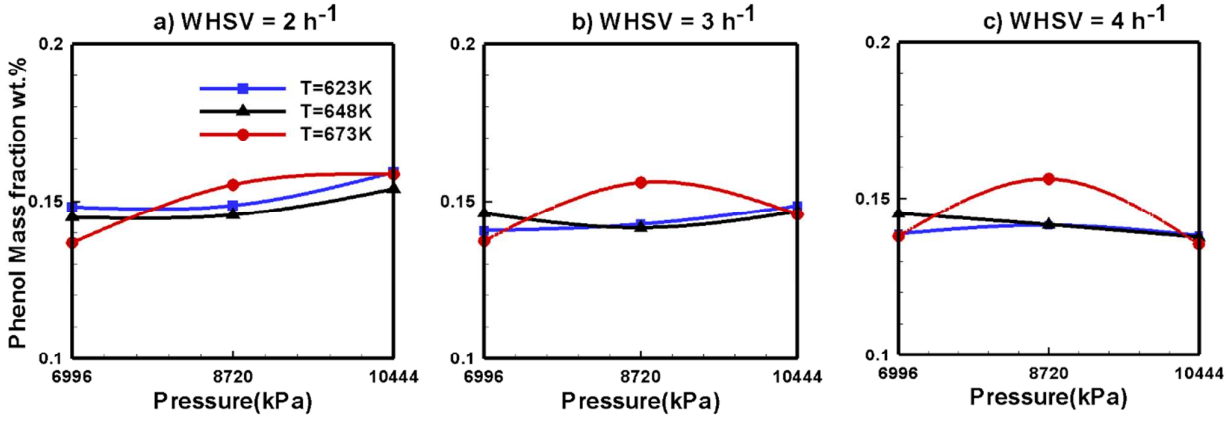

Figure 9 Final steady mass fractions of phenols in the upgraded pine-oil obtained in a fixed bed reactor in the presence of Pt/Al_2O_3 catalyst.

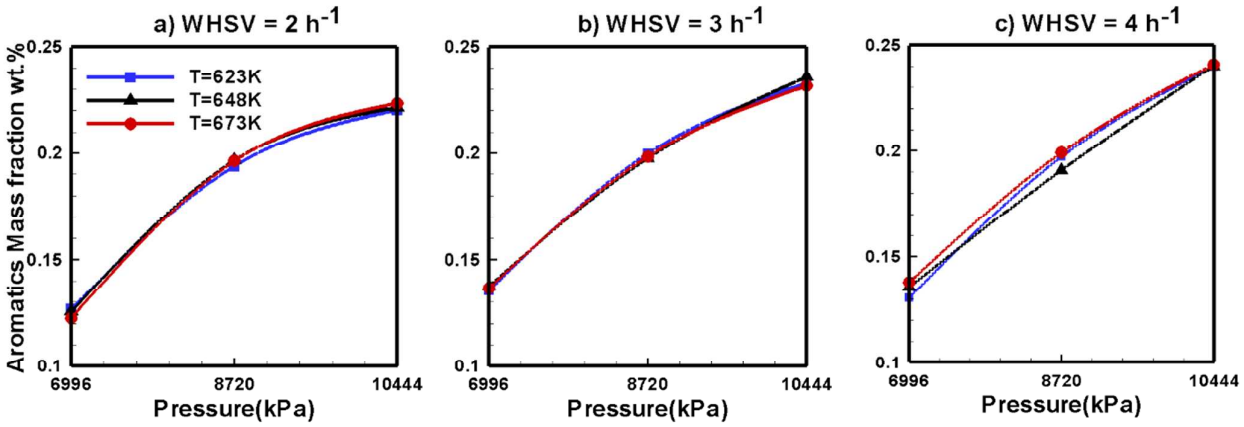

Figure 10 Final steady mass fractions of alkane and aromatics in the upgraded pine-oil obtained in a fixed bed reactor in the presence of Pt/Al_2O_3 catalyst.

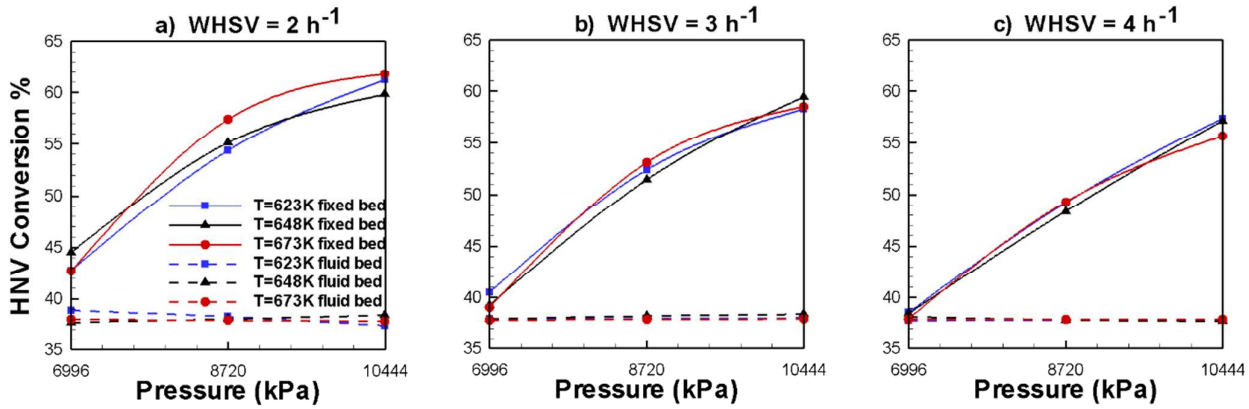

Figure 11 Comparison of conversion of HNV in fixed and fluid bed reactors at different T, P and WHSV values.

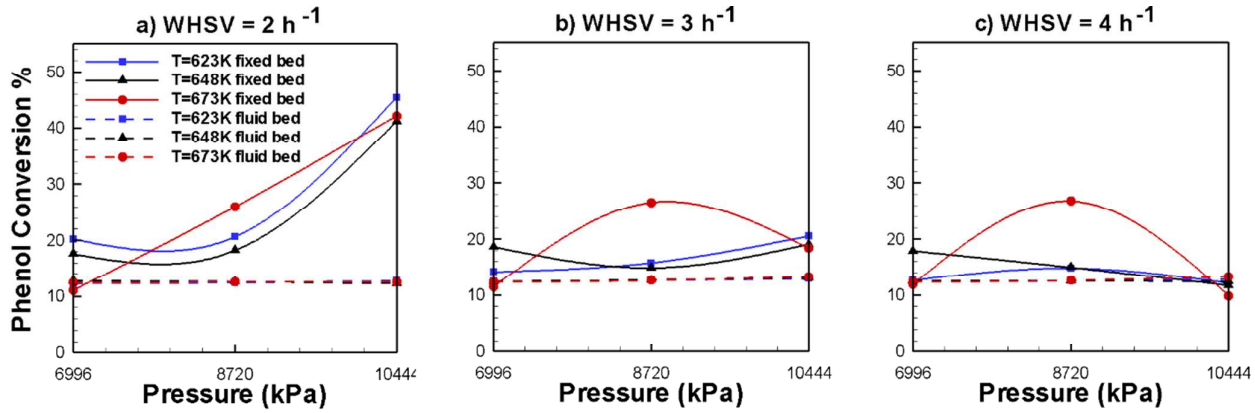

Figure 12 Comparison of conversion of phenols in fixed and fluid bed reactors at different T, P and WHSV values.

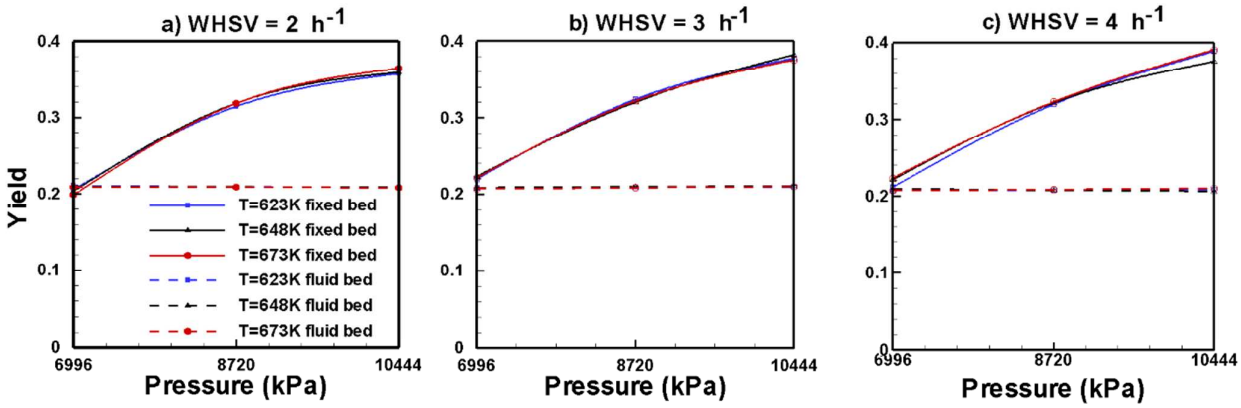

Figure 13 Comparison of yield of alkane and aromatics in fixed and fluid bed reactors as function of T, P and WHSV.

Table 9 Mass fractions of product species with respect to different operating conditions using Pt/Al_2O_3 catalyst in a fixed bed reactor.

Species	WHSV = 2 h^{-1}			WHSV = 3 h^{-1}			WHSV = 4 h^{-1}		
	P = 6996 kPa								
	T = 623 K	T = 648 K	T = 673 K	T = 623 K	T = 648 K	T = 673 K	T = 623 K	T = 648 K	T = 673 K
HNV	0.2822	0.2736	0.2825	0.2935	0.2996	0.3006	0.3031	0.3036	0.3061
LNV	0.4210	0.4261	0.425	0.4303	0.4367	0.4357	0.4275	0.4355	0.4265
Phenol	0.1481	0.1448	0.1368	0.1406	0.1461	0.1373	0.1387	0.1452	0.1379
Alkane+Aromatic	0.1267	0.1254	0.1225	0.1354	0.1475	0.1365	0.1305	0.1455	0.1378
Coke+H_2O+Gases	0.0220	0.0301	0.0332	0.0002	-0.0299	-0.0101	0.0002	-0.0297	-0.0083
	P = 8720 kPa								
HNV	0.2251	0.2214	0.2102	0.2349	0.2396	0.2315	0.2505	0.2546	0.2501
LNV	0.4089	0.4063	0.4083	0.4125	0.4112	0.4194	0.4309	0.4319	0.4398
Phenol	0.1486	0.1456	0.1552	0.1426	0.1415	0.1559	0.1414	0.1416	0.1562
Alkane+Aromatic	0.1938	0.1965	0.1962	0.1998	0.1975	0.1984	0.1971	0.1908	0.1991
Coke+H_2O+Gases	0.0236	0.0329	0.0301	0.0102	0.0102	-0.0052	-0.0199	-0.0189	-0.0452
	P =10443 kPa								
HNV	0.1912	0.1982	0.1884	0.2059	0.2001	0.2047	0.2104	0.2115	0.2189
LNV	0.3692	0.3712	0.3784	0.3781	0.3792	0.3801	0.3902	0.3968	0.4011
Phenol	0.1792	0.1739	0.1751	0.1485	0.1467	0.1458	0.1381	0.1376	0.1354
Alkane+Aromatic	0.2202	0.2214	0.2234	0.2329	0.2357	0.2316	0.2398	0.2402	0.2409
Coke+H_2O+Gases	0.0402	0.0353	0.0347	0.0346	0.0383	0.0378	0.0215	0.0139	0.0037

Conclusions

The upgradation of pyrolytic oil by HDO process in the presence of Pt/Al_2O_3 is numerically studied and some of the key conclusions are as follows. The bed experiences slight expansion at WHSV = 2 h^{-1}. However no expansion of bed observed when WHSV = 3 h^{-1} and WHSV = 4 h^{-1}. The mass fractions of undesirable HNV and LNV in the final pyrolytic bio-oil at steady state are found to substantially decrease with pressure and slightly increase with WHSV while the effect of temperature is very small. On the other, mass fractions of desirable aromatics significantly increases with pressure but slightly increases with WHSV whereas the temperature effect is negligible. Finally conversion of HNV and phenols and yield of alkanes and aromatics in fluid bed reactor are very small and unaffected by operating conditions; whereas in the fixed bed reactor, these conversions and yield are significantly large which further increases with the pressure. Finally it is recommended that the HDO of pyrolytic oil in the presence of Pt/Al_2O_3 is favourable at high pressures in upflow fixed bed reactors than in fluid bed reactors.

Acknowledgements

Authors gratefully acknowledge the support received from Prof. Sai Gu (Centre for Biofuel, School of Energy, Environmental and Agrifood, Cranfield University, UK) in the beginning stage of this project.

References

1. H.B. Goyal, D. Seal, R.C. Saxena, Renew. Sustain. *Energy Rev.* 2008, **12**, 504–517.
2. Q. Zhang, J. Chang, T. Wang, Y. Xu, *Energy Convers. Manag.* 2007, **48**, 87-92.
3. A.V. Bridgwater, *Biomass Bioenergy*, 2012, **38**, 68-94.
4. D.C. Elliott, *Energy and Fuels*, 2007, **21**, 1792–1815.
5. X. Hu, C. Lievens, A. Larcher, C.Z. Li, *Bioresour. Technol*., 2011, **102**, 10104–10113.
6. X. Hu, R. Gunawan, D. Mourant, Y. Wang, C. Lievens, W. Chaiwat, L. Wu, C.Z. Li, *Bioresour. Technol.,* 2012, **123**, 249–255.
7. R. French, S. Czernik, *Fuel Process. Technol*., 2010, *91*, 25–32.
8. A. Aho, N. Kumar, K. Eränen, T. Salmi, M. Hupa, D.Y. Murzin, *Fuel*, 2008, **87**, 2493–2501.
9. J. Wildschut, F.H. Mahfud, R.H. Venderbosch, H.J. Heeres, *Ind. Eng. Chem. Res*., 2009, **48**, 10324–10334.
10. O. Şenol, T.R. Viljava, A.O.I. Krause, *Catal. Today*, 2005, **100**, 331–335.
11. E. Furimsky, *Appl. Catal. A Gen*., 2000, **199**, 147–190.
12. J.R. Galdámez, L. Garcia, R. Bilbao, *Energy and Fuels*, 2005, **19**, 1133-1142.
13. E. Furimsky, *AIChE J.*, 1979, **25**, 306–311.
14. D.C. Elliott, E.G. Baker, *Biotechnol. Bioeng. Symp.* 1984, 14, 159–174.
15. J. Gagnon, S. Kaliaguine, *Ind. Eng. Chem. Res*., 1988, **27**, 1783–1788.
16. Y.E. Sheu, R.G. Anthony, E.J. Soltes, *Fuel Process. Technol*., 1988, **19**, 31–50.
17. D.C. Elliott, G.F. Schiefelbein, *Amer. Chem. Soc. Div. Fuel Chem. Prepr.*, 1989, **34**, 1160–1166.
18. A. Oasmaa, D. Boocock, *Can. J. Chem. Eng*., 1992, **70**, 294–300.
19. W. Baldauf, U. Balfanz, M. Rupp, *Biomass and Bioenergy*, 1994, **7**, 237–244.
20. L. Conti, G. Scano, J. Boufala, S. Mascia, *Bio-Oil Prod. Util.* 1996, 198.
21. M.C. Samolada, W. Baldauf, I.A. Vasalos, *Fuel*, 1998, **77**, 1667–1675.
22. Z. Su-Ping; Y. Yong-Jie, R. Zhengwei, L. Tingchen, *Energy Sources*, 2003, **25**, 57–65.
23. D.C. Elliott, T.R. Hart, *Energy and Fuels*, 2009, **23**, 631–637.
24. M. Saidi, F. Samimi, D. Karimipourfard, T. Nimmanwudipong, B.C. Gates, M.R. Rahimpour, *Energy Environ. Sci.*, 2014, **7**, 103-129.
25. R.P. Divya, K.G. Vamshi, K.P. Venkata, H.S. Philip, S. K. Tanneru, *Environ. Prog. Sustain. Energy*, 2014, **33**, 726-731.
26. L. Schiller, Z. Naumann, *Ver. Deutsch. Ing.*, 1935, **77S**, 318-325.
27. D. Jianmin, D. Gidaspow, *AIChE J.*, 1990, **36**, 523–538.
28. D. Gidaspow, R. Bezburuah, J. Ding, Hydrodynamics of circulating fluidized beds: kinetic theory approach. In: Potter OE, Nicklin DJ, editors. *Fluidization VII:7th Engineering Foundation,* Montreal: McGill University; *1992*, 75-82.
29. C.Y. Wen, Y. H. Yu., *Chem. Eng. Prog. Symp. Series* ., 1966, **62**, 100–111.
30. S. Ergun., *Chem. Eng. Prog*., 1952, **48**, 89–94.
31. C.K.K. Lun, S.B. Savage, D.J. Jeffrey, N. Chepurniy, *J. Fluid Mech.*, 1984, **140**, 223-256.
32. W.E. Ranz, W.R. Marshall, *Chem. Eng. Prog*., 1952, **48**, 141–146.
33. D.J. Gunn, *Int. J. Heat Mass Transf*., 1978, **21**, 467–476.
34. L.R. Stowe, Method of conversion of heavy hydrocarbon feedstocks, *US Pat.*, US5547563 A, 1996.
35. D.J. Raal, A. Muhlbauer, *Phase Equilibria: Measurement & Computation*, Taylor & Francis, Washington, USA, 1997.
36. S.C. Lin, Hydrocarbons via catalytic hydrogen treatment of a wood pyrolytic Oil, PhD Thesis, A & M University, Texas, 1981.
37. Ansys Fluent, Fluent User's Guide, In Fluent Inc, 2006.
38. A.R.K. Gollakota, M.D. Subramanyam, N. Kishore , S. Gu, *RSC Adv*., 2015, **5**, 41855-41866.
39. Y. Wang, T. He, K. Liu, J. Wu, Y. Fang, *Bioresour. Technol*., 2012, **108**, 280-284.
40. J.F. Zhu, J.C. Wang, Q.X. Li, *Chin. J. Chem. Phys*., 2013, **26**, 477-483.

Table of Contents

Hydroprocessing of pine-oil in a fixed bed reactor in the presence of Pt/Al_2O_3 is numerically investigated as function of temperature, pressure and WHSV.